

# Accurate prediction of ecDNA in interphase cancer cells using deep neural networks

Received: 17 June 2025

Accepted: 24 March 2026

Cite this article as: Prasad, G., Rajkumar, U., Curtis, E.J. *et al.* Accurate prediction of ecDNA in interphase cancer cells using deep neural networks. *Commun Biol* (2026). <https://doi.org/10.1038/s42003-026-09982-4>

Gino Prasad, Utkrisht Rajkumar, Ellis J. Curtis, Ivy Tsz-Lo Wong, Xiaowei Yan, Shu Zhang, Lotte Brückner, Kristen Turner, Julie Wiese, Justin Wahl, Homa Hemmati, Sihan Wu, Jessica Theissen, Matthias Fischer, Howard Y. Chang, Anton G. Henssen, Paul S. Mischel & Vineet Bafna

We are providing an unedited version of this manuscript to give early access to its findings. Before final publication, the manuscript will undergo further editing. Please note there may be errors present which affect the content, and all legal disclaimers apply.

If this paper is publishing under a Transparent Peer Review model then Peer Review reports will publish with the final article.

# Accurate Prediction of ecDNA in Interphase Cancer Cells using Deep Neural Networks

Gino Prasad<sup>1,\*</sup>, Utkrisht Rajkumar<sup>1,\*</sup>, Ellis J. Curtis<sup>2,3,4</sup>, Ivy Tsz-Lo Wong<sup>2,3</sup>, Xiaowei Yan<sup>2,3,5,6,7</sup>, Shu Zhang<sup>2,3,6,7</sup>, Lotte Brückner<sup>8,9,10</sup>, Kristen Turner<sup>11</sup>, Julie Wiese<sup>11</sup>, Justin Wahl<sup>11</sup>, Homa Hemmati<sup>11</sup>, Sihan Wu<sup>12</sup>, Jessica Theissen<sup>13</sup>, Matthias Fischer<sup>13,14</sup>, Howard Y. Chang<sup>5,6,7,15,16</sup>, Anton G. Henssen<sup>8,9,10</sup>, Paul S. Mischel<sup>2,3</sup>, Vineet Bafna<sup>1,17,†</sup>

<sup>1</sup> Department of Computer Science and Engineering, University of California San Diego, San Diego, CA, USA

<sup>2</sup> Department of Pathology, Stanford University School of Medicine, Stanford, CA, USA

<sup>3</sup> Sarafan ChEM-H, Stanford University, Stanford, CA, USA

<sup>4</sup> Medical Scientist Training Program, University of California San Diego, San Diego, CA, USA

<sup>5</sup> Center for Personal Dynamic Regulomes, Stanford University, Stanford, CA, USA

<sup>6</sup> Department of Dermatology, Stanford University School of Medicine, Stanford, CA, USA

<sup>7</sup> Department of Genetics, Stanford University School of Medicine, Stanford, CA, USA

<sup>8</sup> Department of Pediatric Hematology and Oncology, Charité-Universitätsmedizin Berlin, Berlin, Germany

<sup>9</sup> Experimental and Clinical Research Center (ECRC) of the MDC and Charité Berlin, Berlin, Germany

<sup>10</sup> Max-Delbrück-Centrum für Molekulare Medizin (BIMSB/BIH), Berlin, Germany

<sup>11</sup> Boundless Bio, San Diego, CA, USA

<sup>12</sup> Children's Medical Center Research Institute, University of Texas Southwestern Medical Center, Dallas, Texas

<sup>13</sup> Department of Experimental Pediatric Oncology, University Children's Hospital of Cologne, Medical Faculty, University of Cologne, Cologne, Germany

<sup>14</sup> Center for Molecular Medicine Cologne (CMMC), Medical Faculty, University of Cologne, Germany

<sup>15</sup> Howard Hughes Medical Institute, Stanford University School of Medicine, Stanford, CA, USA

<sup>16</sup> Current address: Amgen Research, South San Francisco, CA, USA

<sup>17</sup> Halicioğlu Data Science Institute, University of California at San Diego, La Jolla, CA, USA

\* These authors contributed equally to this work.

† Corresponding author: Vineet Bafna: vbafna@ucsd.edu

## ABSTRACT

Oncogene amplification is a key driver of cancer pathogenesis and is often mediated by extrachromosomal DNA (ecDNA). EcDNA amplifications are associated with increased pathogenicity of cancer and poorer outcomes for patients. EcDNA can be detected accurately using fluorescence in situ hybridization (FISH) when cells are arrested in metaphase. However, the majority of cancer cells are non-mitotic and must be analyzed in interphase, where it is difficult to discern extrachromosomal amplifications from chromosomal amplifications. Thus, there is a need for methods that accurately predict oncogene amplification status from interphase cells.

We present interSeg, a deep learning-based tool to cytogenetically classify oncogene amplification status as extrachromosomally amplified (EC-amp), intrachromosomally amplified (HSR-amp), or not amplified, from interphase FISH images. We trained and validated interSeg on 652 images (40,446 nuclei). Tests on 215 cultured cell and tissue model images (9,733 nuclei) showed 89% and 97% accuracy at the nuclear and sample levels, respectively. The neuroblastoma patient tissue hold-out set (67 samples and 1,937 nuclei) also revealed 97%

accuracy at the sample level in detecting the presence of focal amplification. In experimentally and computationally mixed images, interSeg accurately predicted the level of heterogeneity. The results showcase interSeg as an important method for analyzing oncogene amplifications.

## INTRODUCTION

Oncogene amplification is a key driver of cancer pathogenesis<sup>1,2</sup>. Focal oncogene amplifications can occur within specific chromosomes as homogeneously staining regions<sup>3,4</sup> (HSR) or as extrachromosomal DNA<sup>5</sup> (ecDNA). EcDNAs are circular, acentric molecules that replicate independently from linear chromosomes and segregate randomly in daughter cells<sup>6</sup>. EcDNAs are present in a third of all samples, and in two-thirds of cancer subtypes<sup>7</sup>. They are especially frequent in glioblastoma<sup>8</sup>, neuroblastoma<sup>9</sup>, and esophageal carcinoma<sup>5,7</sup>, but have also been detected in pre-cancerous lesions<sup>10</sup>. Compared to other intrachromosomal focal amplifications, ecDNAs are associated with increased pathogenicity of cancer and worse outcomes for patients<sup>7</sup>. Recent commentaries highlight the important need for methods and tools to detect focal amplifications in tumor cells and classify their location as being intrachromosomal or extrachromosomal, both in research studies and in the clinic<sup>11,12</sup>.

In research settings, AmpliconArchitect, JaBbA, and related methods<sup>13–16</sup> have been used to analyze the patterns of whole-genome sequencing reads sampled from a tumor genome and mapped to a normal reference to (a) identify copy number patterns indicative of focal amplification, (b) use focally amplified regions as seeds, and (c) utilize discordantly paired-reads to explore the fine genomic structure of focal amplifications. The presence of discordant reads that represent a cyclic structure is highly indicative of ecDNA structure<sup>7</sup>. These WGS methods have been extended to whole exome<sup>17</sup> and even panel sequencing<sup>18</sup>. Sequence-based methods can reliably distinguish ecDNA from stable chromosomal amplifications (displaying as HSRs) formed by breakage-fusion-bridge cycles and other mechanisms<sup>4</sup>. However, HSRs may also be formed when ecDNA re-integrate into chromosomes in response to the cellular environment<sup>19</sup>. The HSRs formed by re-integrated ecDNA retain their sequence features, making it difficult for sequence-based methods to predict the amplification mechanism.

Fluorescent and DAPI imaging of DNA in metaphase spreads are currently the gold-standard for determining the location (intra- or extrachromosomal) of focal amplification. EcDNAs appear as hundreds of tiny faint DNA particles, detached from the compacted chromosomes seen in metaphase. Fluorescently labeled DNA FISH probes for specific genes can additionally determine if the ecDNAs carry those genes. A deep-learning method, ecSeg, was successfully utilized to semantically segment images of metaphase cells and annotate the pixels representing ecDNA<sup>20</sup>. However, capturing cells in metaphase requires synchronization of cells, which is typically possible only in cultured cell lines. In clinical practice, cells are harvested from patient tumor tissue and readily archived as flash-frozen tissue samples, or as formalin-fixed paraffin-embedded samples. The majority of cells are non-mitotic and must be analyzed in interphase, where the DNA is loosely arranged inside an intact nuclear membrane. This makes it extremely challenging to identify ecDNA, even for a trained eye. Very recently, a method, ecPath<sup>21</sup>, has been developed to identify ecDNA directly from H&E-stained images from cancer tissue sections. It has broad applicability but also utilizes sequence-based methods as a gold standard.

In this work, we discern HSR and ecDNA amplifications using the unique fluorescent staining patterns of amplicons in interphase nuclei. We present interSeg, a deep learning-based tool to cytogenetically determine amplification status of a target FISH probe. interSeg relies on two independent deep learning modules: ecSeg-c and ecSeg-i. EcSeg-c uses centromeric and target FISH probes to determine if the target is amplified. The additional centromeric probe provides a control for aneuploidy, whole genome duplication and overlapping cells, which may result in higher number of FISH foci. EcSeg-i determines the mode of amplification as ecDNA or HSR, assuming focal amplification of the target, and requires only the target FISH probe.

## RESULTS

We modeled ecDNA detection in interphase nuclei as a problem of nuclear classification, where each interphase nucleus was assigned to one of three categories (Figure 1a): amplification on ecDNA ('EC-amp'); intrachromosomal amplification, described by a homogeneously stained region ('HSR-amp'); or no amplification of the target probe ('no-amp'). Each cytogenetic image itself contained a collection of interphase nuclei and were found to have different characteristics depending on the source. Therefore, we first collected representative cytogenetic images from different sources to create a dataset.

### Dataset overview

We used 3 different protocols (Figure 1b) to acquire images from 13 different tissue types (Figure 1c). 'Cultured cells' refer to cells grown outside of their natural environment, typically in a culture, and plated on a slide prior to image acquisition. This results in images with dissociated and sparse nuclei. 'Tissue models' are either cells obtained from xenografts, which are tissues transplanted from human to mouse, then biopsied for image acquisition, or they represent cell lines cultured in vitro, but fixed and paraffin embedded in cell pellets. This results in images with more tightly packed cells. 'Patient tissue' corresponds to tightly packed cells in tissue sections from tumor biopsies (Supplementary Figure 1 and Methods), but may have more heterogeneity and a higher fraction of normal tissue cells. After excluding images that did not achieve a threshold quality score (see Methods), we obtained 231 cultured cell images and 443 tissue model images from 32 unique cell lines, and 265 images from patient-derived neuroblastoma (NB) samples (Supplementary Table 1). The cell lines were chosen based on their prior utilization for investigating focal amplifications in cancer and ecDNA<sup>22,7,23-25</sup> (Supplementary Table 2). In addition, we utilized 60 'mixed' images (765 nuclei) from a special tagging experiment designed to test performance in heterogeneous samples containing both ecDNA and HSR (See Methods).

We used whole genome sequencing (WGS) to identify the amplified oncogene in the cultured cell and tissue model cell lines, as described in earlier publications<sup>7</sup>. We then probed for these amplified genes using FISH probes in DAPI stained metaphase spreads where the chromosomes are compacted, and the nuclear location of the FISH probe can be unambiguously determined. This provided the truth set for whether the oncogene was amplified on ecDNA or HSR<sup>7</sup>. A few cell lines were probed for more than one oncogene (e.g. H716 for *FGFR2* and *MYC*) to obtain 39 unique cell line-oncogene pairs. The cell line-oncogene pairs ( $l, g$ ) from the cultured cell lines and tissue-models were assigned a label  $L(l, g)$  as being one of EC-amp, HSR-amp, or no-amp.

Correspondingly, each nucleus with a fluorescent label for gene  $g$  in an interphase image of cell line  $l$  also received the label  $L(l, g)$ , providing us with a data set of nuclei that could be utilized for training, validation, and testing. For example, we labeled all nuclei in the COLO320HSR cell line as HSR-amp for the oncogene *MYC*.

We trained ecSeg-i and ecSeg-c separately. For ecSeg-i, we performed a 50-50 training/validation hold-out set split on the 231 cultured cell images, and a 75-25 training/validation hold-out set split on the 443 tissue model images. In total, we utilized 459 images (35,096 nuclei) for training/validation, and 215 images for hold-out testing (Supplementary Table 1). Finally, we utilized the NB patient tissue images as analysis sets for biological interpretation (265 images, 7,466 nuclei). Notably, the trained neural networks never accessed the 215 hold-out test images from cultured cells and tissue models, 60 mixed images, or the 265 patient tissue images during training or validation of ecSeg-i.

EcSeg-c requires centromeric and target FISH probes, and it returns a classification of ‘focal-amp’ or ‘no-focal-amp’ for each nucleus. 392 of the 443 tissue model images had a centromeric probe and met our centromeric quality score criterion. We labeled images with HSR-amp and EC-amp classifications as ‘focal-amp’ for ecSeg-c training. Other images were labeled ‘no-focal-amp’. Of the 392 images, 95 images (7,501 nuclei), which were also in the hold-out set of ecSeg-i, were used as a test set to prevent leakage. The remaining 297 images (22,970 nuclei) were used for ecSeg-c training/validation. For our NB patient tissue dataset, 260 of the 265 NB samples met our centromeric quality criterion, and were labeled by pathologists as ‘amplification’, or not. The NB patient tissue image dataset was split 75-25 into training/validation (5,350 nuclei from 193 images) and hold-out set (1,937 nuclei from 67 images).

### InterSeg architecture overview

Recall that interSeg has two distinct modules: ecSeg-i and ecSeg-c, both of which make predictions on individual nuclei annotated with DAPI and FISH. Therefore, we used an available method, NuSeT<sup>26</sup>, to first segment each image into individual nuclei (Figure 2a). These individual nuclei are fed to ecSeg-i and ecSeg-c. Salient features and data filtering issues are described below, with details in methods.

EcSeg-i and ecSeg-c are both based on the DenseNet-121 architecture<sup>27</sup> (Methods). DenseNet-121 is a densely connected network with exhaustive skip connections between convolutional blocks, enabling feature-reuse throughout the network. The feature maps of all previous layers were concatenated and fed as input to the current layer, making it *densely* connected (Figure 2b).

The original DenseNet has a final classification layer with 1000 output nodes, corresponding to 1000 ImageNet<sup>28</sup> classes. In our version of DenseNet for ecSeg-i, we used a final classification layer with 3 output nodes corresponding to the three output classes: EC-amp, HSR-amp, and no-amp. We performed a grid-search to train a DenseNet from scratch, and used the results to select hyperparameters.

Ec-Seg-i returns the posterior probability of the membership in each class as the output for each nucleus. As a post-processing step, it optionally labels each nucleus with the amplification

mechanism with the greatest posterior probability from ecSeg-i. Because there is considerable heterogeneity in ecDNA counts from cell to cell, most scientists make predictions based on groups of cells rather than individual cells. Therefore, we additionally generated cell line level metrics by employing a bootstrapping approach on the results obtained at the nucleus level (Methods). Briefly, this involved selecting 10 cells in each sampling instance and determining the most prevalent amplification mechanism within this group. This process was iterated 100 times, with a random selection of 10 cells in each iteration. The outcome of this iterative process was employed as the cell line level statistics.

EcSeg-i assumes that any amplification of the target is a focal event. However, amplifications can also occur due to aneuploidies, and this can be cytogenetically tested by using a centromeric probe. We trained a separate neural network (*ecSeg-c*) with the same DenseNet121 architecture as ecSeg-i (Supplementary Figure 2). For each nucleus, ecSeg-c predicts a binary classification label, focally amplified or not. We performed extensive training and validation of interSeg modules (Methods and Supplementary Figures 3-8).

As with all deep-learning methods, a direct and intuitive explanation of the ecSeg-i posterior probabilities output is not available. This is specifically confounding for interphase FISH analysis where the high variability from cell to cell makes interpretation difficult even for the trained eye. To improve interpretation, we implemented a second module called *stat-FISH* to gather statistics that provide complementary evidence (Methods). These statistics are not used to change the output of ecSeg-i, but are provided as an addendum to ecSeg-i posterior probabilities. Importantly, in contrast to the per-cell posterior probabilities output by ecSeg-i, *stat-FISH* mimics human interpretation by analyzing and integrating the data from multiple nuclei (Supplementary Figure 9).

### **EcSeg-i and ecSeg-c accurately determine amplification mechanisms**

In cases where a centromeric probe is not available, InterSeg defaults to running ecSeg-i (Figure 2a). Therefore, we tested ecSeg-i and ecSeg-c independently. EcSeg-i was tested on each of the 9,733 nuclei from the 118 cultured-cell and 97 tissue model images in the hold-out test data set. The 9,733 nuclei included 1,539 with no-amp, 3,497 nuclei with EC-amp, and 4,697 nuclei with HSR-amp. The model achieved F1-scores of 0.91 (recall: 0.91, precision: 0.91) for no-amp, 0.87 (recall: 0.91, precision: 0.84) for EC-amp, and 0.88 (recall: 0.86, precision: 0.91) for HSR-amp nuclei at the per-nucleus identification level (Figure 3a). These results are conservative estimates, as they assume uniform amplification within each cell line, despite the expected heterogeneity or lack of amplification in all cell lines.

Next, we tested ecSeg-c. EcSeg-c was trained on the 297 tissue model images and 193 NB patient tissue images and subsequently tested on 95 tissue model images and 67 NB patient tissue images, as described earlier. On the tissue model images, we obtained a nucleus-level F1 score of 0.95 (recall: 0.95, precision: 0.94) and 0.99 (recall: 0.99, precision: 0.99) on the no-amp and amp classes respectively. For the NB patient tissue test subset, ecSeg-c obtained a 0.78 F1 score (recall: 0.92, precision: 0.67) on the no-amp class and a 0.92 F1 score (recall: 0.88, precision: 0.98) on the amp class at the per-nucleus level. For sample-level predictions (Figure

3e), we observed a 0.95 F1 Score (recall: 1.0, precision: 0.90) on no-amp and 0.98 F1 Score (recall: 0.96, precision: 1.0) on amp labels.

Notably, because we did not have metaphase annotations of ecDNA or HSR on the patient tissue images, the combined interSeg could only be tested on the cultured cells and tissue models. On the 118 cultured cell test images and 97 tissue model test images, interSeg obtained nucleus level F1 scores of 0.92 (recall: 0.97, precision: 0.88), 0.87 (recall: 0.91, precision: 0.85), and 0.89 (recall: 0.85, precision: 0.93) respectively for the no-amp, EC-amp, and HSR-amp classes.

InterSeg uses a third-party tool, NuSeT, for segmenting nuclei<sup>26</sup>. For patient tissue images where the cells can tightly pack together, NuSeT may have difficulty segmenting nuclei. To test the accuracy of interSeg on manual vs automated segmentation inputs, we randomly selected 4 NB samples from the hold-out set: two pathologist-annotated 'Amplification' and two 'No Amplification' neuroblastoma samples. We segmented nuclei manually and performed a cell-by-cell comparison of the interSeg predictions between the manually segmented and the NuSeT segmented nuclei. For two samples (DB, DL) in the 'No Amplification' groups, interSeg predicted 94.4% and 100% of nuclei as No-amp using NuSeT segmentation, respectively (Supplementary Data 1). With manual segmentation, both No-amp samples had 100% of nuclei predicted as No-amp. For the pathologist-labeled 'Amplification' samples (CC and KM), 88.5% and 92.9% of nuclei were predicted as either EC-amp or HSR-amp using the NuSeT segmentation, respectively. Using manual segmentation, 94.6% and 88.0% of nuclei, respectively, were predicted as either EC-amp or HSR-amp for samples CC and KM. For sample CC with the largest improvement in accuracy, the hand-annotated segmentation contained 37 individual nuclei compared with only 26 nuclei in the NuSeT segmentation (Supplementary Figure 10). Overall however, the NuSeT predictions were robust. For cultured cells, we observed no difference between automated and manual segmentations.

The bootstrapped version of interSeg was tested 100 times on each of the 39 cell line-oncogene pairs to obtain single predictions for each pair. It correctly predicted the majority of the bootstrapped trials to carry the expected amplification in 38 out of the 39 samples overall (Figure 3b-d). Even in the non-bootstrapped nuclear level predictions, interSeg predicted more than 60% of the nuclei as EC-amp in all 15 ecDNA cell lines, more than 90% of the cells as no-amp in all 3 no-amp cell lines, and at least 50% of the cells as HSR-amp in 20 out of 21 HSR cell lines (Supplementary Figure 11 and Supplementary Data 2).

While bootstrapping eliminates small variability due to mis-prediction or noise, the remaining high variability in certain samples suggested heterogeneity between ecDNA and HSR. For example, the metaphase cell in SF268 shows two HSR amplifications. However, the stat-FISH data shows seven distinct FISH foci with a puncta pattern and an ecSeg-i posterior probability indicative of EC-amp (Supplementary Figure 12). In contrast, Supplementary Figure 13 shows a second SF268 nucleus with a high foci count of 9; in this case, ecSeg-i predicted the nucleus as primarily HSR-amplified due to the non-puncta distribution of the foci. Similar information can be found for SN12C (Supplementary Figure 14).

### **InterSeg determines amplification heterogeneity between cell lines**

To test interSeg prediction performance for heterogeneous samples containing both EC-amp and HSR-amp cells, we first created artificial composite images containing both ecDNA and HSR amplifications by combining the cells in the isogenic lines GBM39EC and GBM39HSR with the FISH probe *EGFR*. For the GBM39HSR cells in the computationally mixed images, we observed a 78%-22%-0% split between HSR-amp, ecDNA-amp, and no-amp predictions respectively. This mirrored the true GBM39HSR prediction percentages, which are 81%-19%-0% respectively. A statistical test could not distinguish between calls made on the pure HSR line versus the HSR labeled cells in the mixed image (chi-square test statistic: 2.3607, P-value: 0.1244). Similarly, for the true GBM39EC cells in the mixed images, we observed a 14%-86%-0% split between HSR-amp, EC-amp, and no-amp predictions respectively. Once again, this could not be statistically distinguished from the pure GBM39EC cell line, where the interSeg predictions were 14%-86%-0% HSR-amp, ecDNA-amp, and no-amp respectively (chi-square test statistic: 0.0186, P-value: 0.8914).

We repeated the experiment after concatenating pairs of test set images from COLO320DM and COLO320HSR with an absolute mean nuclei area difference of less than 50 pixels. This is a harder test because 29% of the cells in the used COLO320DM images were predicted to be HSR with a breakdown of 29%-71%-0% for HSR-amp, ecDNA-amp, and no-amp. Interestingly, the COLO320DM cells in the mixed images also showed a similar 32%-68%-0% distribution for HSR-amp, ecDNA-amp, and no-amp labels, respectively (chi-square test statistic: 1.7475, P-value: 0.1862). Similarly, observed predictions for COLO320HSR cells in the computationally mixed images were 97%-2%-1% for HSR-amp, ecDNA-amp, no-amp, respectively. These matched the interSeg predictions on pure COLO320HSR which were 96%-2%-2% respectively (chi-square test statistic: 0.3706, P-value: 0.8309).

Next, we also tested an experimental system where COLO320DM and COLO320HSR cells were grown on the same plate. An mCherry RFP tag was used to mark COLO320DM cells. A green DNA-FISH probe for *MYC* was used to test amplification in this mixed cell population (Methods). However, we also observed that the RFP tagging accuracy was not 100% and there were a small but unknown number of ecDNA cells that were not tagged (Supplementary Figure 15). Therefore, we utilized a latent parameter  $x$  denoting the number of COLO320DM cells that were not RFP tagged. Next, we computed the optimal value for  $x$  that maximized the likelihood of the observed frequencies seen in the pure cell line test datasets for COLO320DM and COLO320HSR (Methods). At  $x=6.14\%$  (which would imply a tagging accuracy of 93.86%), we observed a strong correlation, or no statistically significant difference between expected heterogeneity and observed heterogeneity (chi-squared test statistic: 2.7252, P-value: 0.4360). Together, these results illustrate the power of interSeg in predicting amplification mechanisms in the presence of heterogeneity.

Based on these results, we decided to use the following rule based on predictions after bootstrapping: A cell line was considered to be no-amp at least 80% of the cells were classified as no-amp; as HSR-amp if at least 80% of the cells were classified as HSR-amp; as EC-amp, if at least 50% of cells were EC-amp. Otherwise, the sample was classified as mixed or heterogeneous.

### **stat-FISH provides an explanation of amplification status.**

Because interSeg uses deep neural networks to determine the amplification mode, there is limited insight into the features used to make this decision (for partial information, see Supplementary Figure 3). Therefore, we analyzed the data with stat-FISH, a complementary module that computes statistics of the distribution of oncogenic foci per cell. As expected, cells with EC-amp had higher mean and variance in the copy number signal compared to HSR-amp cells. Only 40% of the EC-amp images had a mean < 10 and variance < 64, in contrast to 97% of HSR-amp images with those properties (Figure 4a and Supplementary Data 3). The number of foci and the total FISH signal were also significantly higher in EC-amp cells, whether analyzed across all cell lines (Figure 4b,c) or for individual pairs (e.g., Figure 4d and Supplementary Data 4, 5, 6). Despite these differences, there was high variability in the number and spread of FISH foci across samples. The maximum accuracy of stat-FISH amplification status prediction on the test samples, across different cut-offs of mean and variance, was 83%, lower than the 97% sample accuracy of interSeg (Supplementary Table 3 and Methods). Thus, while stat-FISH is a useful complementary method that allows for an intuitive understanding of amplification modes, it lacks the predictive power of the deep neural network of interSeg, which may be correcting for signal-to-noise ratio, changing morphologies, and latent correlations.

### **stat-FISH allows for exploratory quantification of multiple oncogenes.**

While stat-FISH cannot predict amplification status with as much accuracy as interSeg, it nevertheless provides the flexibility for additional computations that are not easy with interSeg. For example, we used stat-FISH to investigate H716, a colorectal cancer cell line where interSeg predicted EC-amp for two distinct probes, corresponding to *FGFR2* and *MYC*, for each investigated cell (Figure 4e and Supplementary Table 4). The included metaphase in the figure confirms the correctness of the two predictions as being distinct ecDNA. We next quantified the FISH signal using stat-FISH. The average and median copy number signal for *FGFR2* was at 10 and 9, respectively, similar to those of *MYC*, which were 9 and 10, respectively. Similar to metaphase, we also found examples of co-occurring *FGFR2* and *MYC* amplification signals that showed up as yellow (*FGFR2*-green and *MYC*-red). The stat-FISH results suggested a higher count of *FGFR2* ecDNA relative to *MYC*, and the individual numbers were significantly higher than co-occurrences (Figure 4f). However, the co-amplification signal was also strong, and significantly higher relative to chance occurrence (Mann-Whitney U test P-value 1.6E-08; Methods). This result suggests either that the ecDNA species interact<sup>23,29</sup> or the existence of ecDNA that carry both *MYC* and *FGFR2*.

### **InterSeg determines heterogeneity of ecDNA in patient tissue samples.**

Across the 265 patient tissue NB samples, the interSeg predictions were 167 EC-amp (63%), 65 as no-amp (25%), and 33 heterogeneous (12%) (Supplementary Data 1). These samples were previously classified by pathologists as 'amplification' or not (Figure 5a), where 'amplification' included the EC-amp, HSR-amp, and heterogeneous calls made by InterSeg. Among the 71 pathologist annotated 'no amplification' samples, interSeg labeled 63 (89%) as no-amp, 5 (7%) as heterogeneous, and 3 (4%) as EC-amp. When limited to the test samples, interSeg called 15

of 18 (83%) as no-amp, and 3 (17%) as heterogeneous (Supplementary Figure 17). Similarly, among the 194 pathologist annotated 'amplification' category, interSeg labeled 164 samples (85%) as EC-amp, 28 (14%) as heterogeneous, only 2 (1%) as no-amp. When limited to the test samples, interSeg called 41 of 49 (84%) as EC-Amp, 7 as heterogeneous (14%), and only 1 (2%) as no-amp.

Because the pathologists used a binary classification between focally amplified or not, we also tested the majority call. On the hold-out NB test data from no-amplification category, interSeg called the majority class as no-amp in 18 (100%) of 18 samples. Similarly, in the focal amplification test data, interSeg called the majority class as amplified in 46 (94%) of 49 samples. Moreover, 43 of the 46 focal amplification calls were labeled as EC-amp, consistent with the high prevalence of ecDNA in *MYCN* amplified neuroblastoma samples<sup>30</sup>. Thus, the interSeg results were highly consistent with pathologist annotations, but provided additional information in terms of cellular heterogeneity, and mode of amplification.

To further validate interSeg's prediction accuracy, we gathered a set of hold-out NB test samples where whole genome sequencing (WGS) data had been acquired. After filtering for quality score and removing samples with fewer than 5 nuclei, 11 NB samples remained (Supplementary Table 5). The Amplicon Suite pipeline (AS) is routinely used to identify ecDNA using WGS<sup>7,31</sup>. Upon analyzing the WGS data with AS, 10 samples were predicted to be cyclic, indicative of ecDNA containing *MYCN*, and 1 showed no focal amplification.

9 of the 10 AS predicted ecDNA samples were also predicted by interSeg to be EC-amp (Figure 5b). For the one remaining AS predicted ecDNA sample, interSeg predicted heterogeneity, with 49% of nuclei as HSR-amp, 42% of nuclei as EC-amp, and 9% of the nuclei as No-amp. The results are highly concordant, because AS makes a single call based on bulk sequencing, and ecDNA have been previously observed to reintegrate into a non-native chromosomal location. One sample was predicted by AS as carrying no focal amplification, and interSeg predicted 100% of the nuclei as no-amp.

## DISCUSSION AND CONCLUSION

Cytogenetically identifying the amplification mechanism in interphase cells is an important and incompletely understood problem. Although methods such as AmpliconSuite can reconstruct focal amplifications from bulk sequencing, they cannot fully capture the dynamics of cell-to-cell heterogeneity in copy number or detect ecDNA reintegration<sup>32,33</sup>. Image-based tools can accurately reconstruct ecDNA in fluorescently stained images of cells in metaphase in which the ecDNA is clearly visible as tiny chromatin bodies floating separately from the chromosomes. However, this requires sampling of cultured or mitotic cells, and is difficult to obtain from patient tissue images<sup>34</sup>. Patient tissue images primarily contain densely clustered interphase cells, where the DNA is inside an intact nuclear membrane and not condensed. Moreover, ecDNA counts vary from cell to cell and include many cells with low counts<sup>8,35,36</sup>. This makes it extremely challenging to discern ecDNA even for a trained eye. Large numbers of FISH foci and heterogeneity of foci number across cells are often taken as evidence for ecDNA<sup>37,38</sup>. Thus, multiple studies have reported ecDNA in primary samples after analyzing whole genome data, and provide anecdotal

examples of the presence of ecDNA or HSRs using interphase FISH images of a small number of cells. We developed the current version of interSeg primarily for research use in these settings. Exploiting these signals on multiple data sets including cultured cells, tissue models, and patient tissue, and on experimentally and computationally mixed cells containing both ecDNA and HSR amplification, interSeg was able to predict heterogeneity accurately, and works well in models of tissue slices.

We also present a companion method, stat-FISH, that provides interpretability to interSeg results and provides useful statistics for deeper analysis. We demonstrated various use cases of interSeg+stat-FISH in predicting amplification status, amplification heterogeneity between EC-amp, HSR-amp, and no-amp cell lines, and reconstructing the amplification profile of multiple oncogenes within a single cell. Most importantly, we show that interSeg accurately quantifies the amplification mechanism of patient tissue images.

InterSeg is flexible enough to use without a centromeric probe, but we recommend using it with a centromeric probe. Also, it is run in an optional bootstrap mode, which smooths the nuclei results through a voting mechanism. The bootstrap mode is best utilized in situations where no heterogeneity is expected, and a single label can be applied to the entire image. In the presence of heterogeneity, interSeg should be run in a non-bootstrapped mode. In the manuscript, we utilized the non-bootstrapped mode for analysis of patient tissues and the heterogeneity experiments, but provided data on both bootstrapped and non-bootstrapped runs.

Many common oncogenes, such as *MYC* and *MYCN*, are known to amplify both as ecDNA or HSRs in different samples<sup>39</sup>. This raises the interesting question of heterogeneity, where the same sample may contain some cells with ecDNA amplifications and other cells with HSR amplifications<sup>40</sup>. Heterogeneity is an important but understudied issue in ecDNA biology. The problem is technically challenging because random segregation and resulting heterogeneity of ecDNA numbers can cause some cells to lose ecDNA. In this study, we demonstrated interSeg's power to detect heterogeneity using controlled experiments with computational and experimental mixtures of cells containing ecDNA and HSRs. Based on the results, we developed a heuristic for determining if a sample was heterogeneous. Across the 265 patient tissue NB samples, interSeg conservatively predicted 33 samples (12%) as heterogeneous. Notably, heterogeneity can also take the form of single cells containing both HSR and ecDNA<sup>40</sup>. In such cases, interSeg will label those cells as ecDNA amplified. Future work will reveal the phenotypic behavior of heterogeneous samples, although we speculate that they will be more similar to ecDNA amplifications.

We note that estimation of the number of ecDNA per cell can be impacted by aneuploidy. Tumor cells that show whole-genome doubling or aneuploidy can show multiple foci after imaging and may show heterogeneity when imaged together with other subclones. Previously, Roukous et al. had observed that the integrated DAPI intensity can be used to determine the cell cycle phase<sup>41</sup>. We followed their approach but did not find evidence of characteristic peaks in the data suggestive of either chromosomal replication or aneuploidy. In future work, we plan to study this effect further in more controlled conditions by choosing cell lines where the aneuploidy status is known and choosing a DAPI imaging protocol with more sensitivity to aneuploidy/chromosomal replication alterations.

Even though we use a unified model for cultured cells, tissue models, and patient tissue, the three modes are quite different. Especially, patient tissues often contain multiple cell types, including normal cells. Currently, interSeg does not correct for tumor purity. Additionally, it uses a third party tool to separate individual nuclei, but may not be able to adequately separate tightly packed nuclei, which in turn could influence the predictions of the number of FISH foci, and the amplification mechanism. In future work, we will experiment with interphase cultured cells where cells are cultured on a cover slip and are not perturbed by any chemicals, to better match the nuclear distribution of ecDNA on patient tissues. InterSeg corrects for problems due to contrast and other quality control issues but more data will be needed to understand the degradation of performance on lower quality data sets.

While interSeg was currently developed for use in a research setting, we plan to adapt it to clinical settings in the future. Currently, pathologists do not distinguish between HSR and EC-amp, making it difficult to experimentally validate the amplification mode (ecDNA/HSR) on patient tissue. Moreover, whole genome sequencing signatures from bulk cells also cannot distinguish ecDNA from HSRs formed by reintegration of ecDNA into the chromosomes while maintaining their structural features. An important example is a clinical test of *HER2* gene amplification, measured using FISH, and the corresponding *HER2* expression measured using immunohistochemistry. Examples of concordance and discrepancy have been observed between these two tests<sup>42</sup>. Adding the amplification context (ecDNA or HSR) using interSeg could provide better contextualization and perhaps a mechanistic explanation for the discrepancy. These are all areas of development which will be addressed in ongoing and future work. Despite these challenges, interSeg has been successfully applied to hundreds of patient tissue images, and should be a useful tool for analysis of focal amplification mechanisms.

## METHODS

### Image Acquisition Protocols

To generate the cultured cell images, we arrested the cells by treating them with Colcemid (Karyomax) at a final concentration of 0.1  $\mu\text{g}/\text{mL}$  for 1-5 hours. Cells were collected, washed with PBS, and re-suspended in 75 mM KCl for 10-15 minutes at 37 °C. The hypotonic buffer reaction was quenched by adding an equal volume of Carnoy's Fixative (3:1 Methanol:Glacial Acetic Acid). Cells were centrifuged, washed, and re-suspended in Carnoy's fixative three more times. They were then re-suspended in 100-400  $\mu\text{L}$  of Carnoy's Fixative and dropped onto non-overlapping sections of humidified slides. Slides were equilibrated in 2x SSC and dehydrated in an ascending alcohol series of 70%, 85%, and 100% ethanol for two minutes each. The appropriate DNA FISH (Empire Genomics) probe was added to the sample and placed on a 75 °C slide moat for 3-5 minutes to melt the DNA. Probe hybridization occurred at 37 °C in a humidified slide moat for 4 hours to overnight. Slides were washed for two minutes each in 0.4x SSC and 2x SSC/0.1% Tween-20. Slides were stained with DAPI, washed in 2x SSC and ddH<sub>2</sub>O, and then mounted with mounting media (ProLong Gold or Vectashield). Cover slips were sealed with clear nail polish to prevent drying of the sample. Images were captured using a 63x objective on either an Olympus BX43 wide-field fluorescent microscope or a Leica Thunder Imager.

The tissue model cells are FFPE samples and obtained either from mouse xenografts or FFPE-embedded cell lines. We have uploaded the metadata for all tissue model images on Mendeley Data (see “Data Availability”). We have outlined the protocol for both methods below.

**Tissue model images derived from cell line xenografts.** The animal experiment protocol was approved by and performed in full accordance with the Institutional Animal Care and Use Committee at Stanford University (IACUC protocol number: 34041). Animals were housed in a conventional barrier facility (located at ChEM-H and Neurosciences Building) on a 12-hour light/dark cycle with access to water and food, and their health status was monitored throughout the course of the experiment. COLO320DM and COLO320HSR were cultured in vitro with DMEM (Corning, #10-013-CV) supplemented with 10% fetal bovine serum and 1% penicillin-streptomycin-glutamine (Gibco). Cells were resuspended in 100 $\mu$ L of 1XPBS:Matrigel Matrix (Corning) mixed in 1:1 ratio. The cell suspension was injected subcutaneously into the flanks of female Foxn1nu nude mice of age 6 weeks using 25 gauge needle syringes. Tumors of around 50mm<sup>3</sup> in size were formed after two weeks and the xenograft-bearing mice were subjected to humane sacrifice when tumor volume reaches approximately 150mm<sup>3</sup>. Cell line xenografts were excised from the mice and fixed immediately in 10% formalin overnight. The samples were then prepared into formalin-fixed paraffin-embedded blocks and sectioned to 5 $\mu$ m thickness onto frosted microscopy slides for downstream DNA FISH staining and analysis.

**Tissue model images derived from FFPE embedded cell lines.** The CytoCell Tissue Pretreatment Kit (LPS 100, Oxford Gene Technology IP Ltd.) was used for heat pretreatment of Formalin-Fixed, Paraffin-Embedded (FFPE) tissue prior to Fluorescence In Situ Hybridization (FISH). All FISH probes were purchased from Empire Genomics Inc. FFPE slides were baked at 50 °C overnight, deparaffinized three times with xylene (1330-20-7, Millipore Sigma) for 10 minutes each, and immersed in 100% and 70% ethanol (64-17-5, VWR International LLC) for 2 minutes each. After washing in water for 2 minutes, the slides were incubated in a pretreatment solution at 100 °C for 40 minutes. Slides were dehydrated in a graded ethanol series of 70%, 85%, and 100%, and then air-dried. Next, 10  $\mu$ L of probe mixture was applied to the hybridization area, cover-slipped, and sealed with CytoBond coverslip sealant (2020-00-1, SciGene Corp.). Slides were incubated in the ThermoBrite System (Abbott) at 80 °C for denaturation and hybridized at 37 °C for 16 hours. After gently removing the coverslip sealant, the slides were immersed in 2x SSC/0.1% Tween-20 (V4261, Promega Corp.) for 3 minutes in the dark. The coverslips were slipped off the slides while still in the SSC buffer. Next, slides were washed in 0.4x SSC solution at 73 °C for 2 minutes, transferred to water for 1 minute, air-dried in darkness, and stained with DAPI (DFS500L, Oxford Gene Technology IP Ltd.), and cover-slipped. FISH results were examined with a Keyence fluorescence microscope (BZ-X800 model, Keyence Corp.).

### Data pre-processing

We pre-processed the images by delineating each individual intact nucleus in the image. We used a package called NuSeT<sup>26</sup> to identify and segment each nucleus. NuSeT utilizes multiple neural networks to identify and separate each nucleus, even in dense, overlapping clusters. We drew a bounding box around each unique nucleus, cropped the region to the bounding box, and resized

the crop to a 256 by 256 patch (Figure 2a). For bounding boxes larger than 256 by 256 pixels, we applied a sliding window approach to obtain multiple 256 by 256 patches, with each patch analyzed separately.

For the ecSeg-c model, each input patch contains channels corresponding to the DAPI probe, centromeric probe, and target probe. To control for the variation in brightness between channels, we uniformly rescaled the DAPI channel to the range 0 to 1. Additionally, we jointly rescaled the target and centromeric probe to the range 0 to 1.

### EcSeg-i and ecSec-c architecture

The backbones of ecSeg-i and ecSeg-c are the DenseNet-121 architecture<sup>27</sup>. Densenet-121 is a 121 layered convolutional neural network (CNN) with 12 layers. The feature maps of all previous layers are concatenated and fed as input to the current layer, making it *densely* connected. The primary benefit of this dense connection is that it enables deeper layers to reuse features learned in earlier layers without having to relearn them. Consequently, a DenseNet uses fewer parameters than an equivalent vanilla CNN.

EcSeg-i and ecSeg-c are composed of four dense blocks containing, 6, 12, 24, and 16 convolutional blocks, respectively. Each convolutional block is composed of 6 sequential operations: batch normalization (BN), a rectified linear unit (ReLU),  $1 \times 1$  convolution, BN, ReLU, and a  $3 \times 3$  convolution. The dimensions of all the feature maps within a dense block are kept the same (i.e. no down-sampling) but the number of filters increases by a growth factor  $k = 32$ . This makes it practical to concatenate the feature maps instead of summing them.

Each convolutional block adds 32 additional feature maps. In total, DenseNet-121 has one  $7 \times 7$  convolutional layer, 58  $3 \times 3$  convolutional layers, 61  $1 \times 1$  convolutional layers, 4 averaging pooling layers, 1 max pooling layer, and one fully connected layer.

The original DenseNet-121 used a final classification layer containing 1000 output nodes as it was trying to classify 1000 classes. For the ecSeg-i model, we use a final classification layer containing 3 output nodes corresponding to the three output classes: EC-amp, HSR-amp, and no-amp. For the ecSeg-c model, we use a final classification layer with 2 output nodes, corresponding to the no-amp and Amp output classes.

### Training Procedure

We trained both the ecSeg-i and ecSeg-c models on 4 GeForce GTX 1080 Ti GPUs using the Adam optimizer. For ecSeg-i, we used a patience criterion of 7, and a learning rate of  $5e-4$ . If the validation loss did not improve for 7 epochs the training was halted. We minimized the cross-entropy loss function to train our network. We trained the network for 200 epochs and found that the model converged after 120 epochs. To find the optimal architecture, we performed a grid-search of the following hyperparameters (see “Grid Search” below).

When training the ecSeg-c model, we initialized the network with the DenseNet121 weights pretrained on the ImageNet dataset. We used a patience criterion of 7 epochs, with the validation

set area under the curve (AuC) metric as the early stopping criterion. Additionally, we used the Adam optimizer with a learning rate of  $5e-4$ , and minimized the binary cross-entropy loss. To control for class imbalance, we applied balanced sampling during each epoch across each tissue type (tissue model/patient tissue) and amplification type (no-amp/amp) pair. We assigned equal sampling weight to each of the 4 tissue type pairs, effectively downsampling the majority classes. We trained the ecSeg-c network for 200 epochs and observed the model converge after 18 epoch. We noted that less training epochs were needed for convergence due to the use of pretrained initial weights. Similar to ecSeg-i, we performed a grid-search for the used hyperparameters.

### Grid Search

Both the ecSeg-i and ecSeg-c models have a DenseNet-121 architecture, which contains:

- A. Initial Convolution and Max Pooling Layers
- B. Dense Blocks and Transition Layers
- C. A Global Average Pooling Layer
- D. Two Fully Connected (Feed-Forward Layers)
- E. The Activation Function (Softmax for ecSeg-i and Sigmoid for ecSeg-c)

Parts A, B, C, and E are fixed in the architecture and do not contain optimization hyperparameters in the grid search. For part D, we set the feature dimension of the first fully connected layer output, also known as the hidden dimension size, as a hyperparameter in the grid search.

In addition to optimizing for the hidden dimension size, we optimized for training hyperparameters, which included batch size and learning rate. In our final models for ecSeg-i and ecSeg-c, we used a hidden dimension size of 128, as this minimized validation loss in the grid search. More details on the grid search and hyperparameters used can be found in Supplementary Tables 6, 7.

### Validation of interSeg modules

We inspected what the architecture learned by visualizing the  $7 \times 7$  filters of the first convolution layer and their corresponding feature maps over a test image. We observed that the majority of the filters initially learned to detect small circular objects, indicative of ecDNA patterns (Supplementary Figure 3). The corresponding feature maps show that the network is able to immediately separate the ecDNA-like structures from the background noise, affirming that the network is learning to recognize the object of interest.

We tested the robustness of interSeg predictions to variation of image acquisition, by artificially distorting the images (see “Image Distortion” below), including shrinking, enlarging, and rotating (Supplementary Figures 4-6). In each case, the performance remained similar or identical to the non-distorted case. We also tested interSeg after changing contrast (Supplementary Figures 7-8), which can seriously impact intensity of the fluorescent signal. In a good image, we expect to see a bimodal distribution for the oncogenic FISH signal with a vast majority of pixels with very low intensity, and a small number of ‘true’ pixels with high intensity reflecting real probe hybridization. Lowering the contrast did not change the bimodality, but raising it led to significant bleeding of the FISH signal, impacting performance for HSR-amp lines but not EC-amp lines (Supplementary Figures 7-8). We used this result to generate a quality score for each image (see

“Quality Score Filtering” below). Three of the tissue model test images were marked as low quality based on this method and were removed from final evaluation. Notably, the patient tissue samples were used only for hold-out testing of ecSeg-i. There were a total of 388 NB patient tissue images, and 283 of these images had a pathologist annotation of ‘amplification’, or ‘no-amplification’. Of these 283 NB images, 265 passed our automated quality score threshold and were used for the testing of ecSeg-i.

We also observed some images with a weak but uniform centromeric signal (high kurtosis of mean nucleus centromeric intensity), in contrast with other images where there was a distinct centromeric signal, with high but varying intensity (low kurtosis). We excluded images with a kurtosis value greater than 3 from our analysis of ecSeg-c. For these images with low centromeric channel quality, only ecSeg-i was used to make calls and ecSeg-c was not run. Additionally, we also defaulted to ecSeg-i when the maximum nucleus centromeric intensity was less than 10 (using a 0-255 scale), as these nuclei contain little centromeric signal. Of the 265 NB samples, 5 failed these centromeric quality score criteria, leaving 260 samples remaining. 67 were set aside as a hold-out test set for ecSeg-c, and 193 were used for training and validation.

### **interSeg bootstrapping of cell predictions**

We note that each experiment typically contains several images. For example, Figure 3b contains 933 viable cells across 6 images of the DLD1 cell line with *MYC* staining. Similarly, we found 368 viable cells across 6 images of the NHDF cell line with *MYC* staining. To address variation in cell and image counts, we applied a custom bootstrapping approach as follows. First, we assigned a single amplification mechanism for each cell based on the highest likelihood prediction from interSeg. Next, our procedure randomly selected 10 cells and identified the predominant amplification mechanism based on the majority vote. We iterated this process 100 times to produce a distribution representing the overall amplification mechanism of the experiment. The original interSeg calls are also retained for comparison, etc.

### **Quality Score Filtering**

For each image, we generate an oncogenic probe quality score which indicates whether the image is apt for interSeg. We first bin the oncogenic FISH signal into 50 buckets based on their pixel intensities. We then find the highest peak left of the 25th bin and right of the 25th bin. We find the peaks by simply comparing the neighboring values. We compute the quality score,  $Q$ , by dividing the leftmost peak ( $h_1$ ) by the rightmost peak ( $h_2$ ),  $Q = h_1/h_2$ . Images with  $Q < 0.2$  were marked as low quality. Additionally, we excluded nuclei with a mean oncogenic FISH signal below 0.05 from both the interSeg and ecSeg-c analyses, as these nuclei exhibited extremely low oncogenic FISH signal.

We generated a centromeric probe quality score for each image as well, based on the kurtosis of the mean centromeric intensity per nucleus. Images with a kurtosis value greater than 3 were marked as having low centromeric probe quality and were excluded from ecSeg-c analysis, defaulting to evaluation in interSeg target-channel-only mode. Additionally nuclei with maximum centromeric pixel intensity less than 10 were also excluded from ecSeg-c analysis and defaulted to the ecSeg-i prediction.

## stat-FISH Segmentation Preprocessing

We employed instance segmentation to decrease the occurrence of overlapping nuclei receiving an inflated foci count. We utilized the min-cut algorithm to transform the binary segmentation output from NuSeT into an instance segmentation. To separate overlapping nuclei, we generated a 4-connectivity pixel graph for each connected component in the NuSeT segmentation. To identify nucleus centers, we applied an L1 distance transformation to the NuSeT segmentation and selected local maximums with greater than a 10-pixel distance away from the nearest background pixel. For a given connected component, we determined the minimum number of edges to be removed to isolate two centers in the pixel graph. We applied this algorithm to all connected components exceeding 1.25 times the median connected component area and separated them based on a flow limit of 60. This preprocessing method was only used for stat-FISH and not interSeg, since stat-FISH outputs a quantitative rather than categorical prediction.

## stat-FISH

Stat-FISH looks for local peaks in brightness in the FISH channel. The input for stat-FISH is a single 8-bit FISH-probe channel, and its corresponding binary image representing the nuclei segmentation from NuSeT. To establish whether a given pixel is classified as an foci (local peak), we have three criteria:

1. The local brightness of the region surrounding the pixel must be greater than the pixel neighborhood
2. The pixel brightness must be greater than a minimum brightness ( $b_{min}$ ).
3. Classified foci must have a minimum size given by ( $s_{min}$ )

This model makes two assumptions:

1. An isolated FISH amplification resembles an isotropic 2d Gaussian, with a diagonal covariance matrix and standard deviation given by  $\sigma$ , a preset parameter to the model.
2. For a given pixel ( $x_0, y_0$ ) in a FISH amplification, the relative intensity of the local pixel neighborhood can be approximated with

$$intensity(x, y) = ce^{-\frac{(x-x_0)^2 + (y-y_0)^2}{2\sigma^2}} + d$$

Let  $\vec{g}$  be a flattened gaussian kernel, and  $\vec{v}$  be a flattened  $n \times n$  pixel neighborhood in the image. The goal is to find the best approximation for  $\vec{v}$  in the subspace spanned by  $\{\vec{g}, \vec{1}\}$ . Using Gram-Schmidt orthogonalization, the orthonormal vectors of this subspace are  $\{\vec{g}_\perp, \frac{1}{n}\vec{1}\}$

Where  $\vec{g}_\perp = \text{normalized}(\vec{g} - (\sum_{i=1}^{n^2} \frac{g_i}{n})\vec{1})$

The best approximation for  $\vec{v}$  is  $c\vec{g}_\perp + \frac{d}{n}\vec{1}$  with  $c = \vec{v} \cdot \vec{g}_\perp, d = \vec{v} \cdot \frac{1}{n}\vec{1}$

Using criteria 1 and 2, we state that for a pixel to be classified as a FISH-foci:

1.  $v \cdot g_\perp \geq c_{min}$ , where  $c_{min}$  is a parameter to the model.  $v$  is the flattened pixel neighborhood surrounding  $(x_0, y_0)$ .

2.  $intensity(x_0, y_0) \geq b_{min}$ , where  $b_{min}$  is a parameter to the model and represents the minimum brightness.

Therefore, to filter for pixels with a local brightness greater than the surrounding neighborhood, we convolve the image (using valid zero-padding) with the 2-d vector  $g_{\perp}$ , and threshold by  $c_{min}$ . Additionally, we threshold the original image by  $b_{min}$  and find the intersection with the  $c_{min}$  thresholding. The number of foci returned for a given cell is the number of connected components in the thresholded 2d array where the connected component pixel size is  $\geq s_{min}$ . To estimate copy number for a given nucleus, we calculated the ratio of the number of oncogenic foci pixels by the total nucleus pixel area as a percentage. This corresponds to the total area of the oncogenic FISH amplifications per nucleus normalized by nucleus area.

We emphasize that stat-FISH is a deterministic tool and primarily quantifies the visual data in the image. It does not accurately determine the amplification mechanism in every case. However, it is useful to understand the interSeg predictions, and is used in conjunction with interSeg.

### Image distortion

We tested the robustness of interSeg by testing against distorted images, including enlarging, shrinking, rotating, and modulating their contrast (Supplementary Figures 4-6). We chose one image from an EC-amp cell line (CCFSTTG1) and one from an HSR-amp cell line (KATOIII). For each image, we shrunk them by 80%, enlarged to 1.2x the original size, rotated them 45 degrees, decreasing the contrast by 40%, and increasing the contrast by 40%.

### Red Fluorescence Probe tagging for generating heterogeneous samples containing ecDNA and HSR.

The COLO320DM and COLO320HSR cell lines used in the study are clones with comparable *MYC* copy numbers, selected from cells obtained from ATCC. COLO320DM H2B-mCherry was engineered by lentiviral infection of H2B-mCherry into isogenic COLO320DM cells, followed by sorting of mCherry-positive cells. Two rounds of cell sorting were performed to ensure that about 95% of the COLO320DM H2B-mCherry line were mCherry-positive.

COLO320HSR and COLO320DM H2B-mCherry cells were cultured in DMEM supplemented with 10% FBS and penicillin-streptomycin. Approximately  $1 \times 10^6$  cells from each cell line were harvested at ~70–80% confluency and fixed with 4% paraformaldehyde (PFA) in PBS for 10 minutes at room temperature, followed by two washes with 1x PBS. The fixed COLO320HSR and COLO320DM H2B-mCherry cells were mixed at a 1:1 ratio and cytopun onto glass slides at 800 rpm for 8 minutes in low mode using a Cytospin 4 centrifuge (Thermo Scientific).

Immunofluorescence (IF) of mCherry was performed on the slide to distinguish between COLO320HSR and COLO320DM H2B-mCherry cells. Slides were permeabilized with 0.5% Triton X-100 in PBS for 15 min at room temperature and blocked with 3% BSA in PBST (PBS + 0.1% Tween-20) for 1 h. Samples were incubated overnight at 4 °C with monoclonal anti-mCherry antibody (clone 16D7, Thermo Fisher, M11217, 1:400), washed with PBST, and incubated with Alexa Fluor-conjugated secondary antibodies (1:500, Thermo Fisher) for 30 min at room

temperature. After washing, cells were post-fixed in 4% PFA for 20 min. DNA FISH targeting MYC (Empire Genomics, Cat. #16399) was performed following IF. Slides were washed twice with PBS and once with 2× SSC, followed by serial dehydration in 70%, 85%, and 100% ethanol. Hybridization was carried out with the MYC probe (1:10 dilution) after denaturation at 80 °C for 20 min, followed by incubation at 37 °C overnight (~16 h). Post-hybridization washes were performed with 0.4× SSC (2 min at room temperature), two rounds of 2× SSC + 0.1% Tween-20, and one wash with 2× SSC. Nuclei were counterstained with Hoechst (1 µg/mL, Thermo Fisher) and mounted in ProLong Gold Antifade Mountant (Thermo Fisher). Images were acquired using a Leica SP8 LIGHTNING confocal microscope with a 63× oil immersion objective (NA 1.4).

### Estimation of RFP Tagging Accuracy in Hybrid COLO320 Experiment

Our goal in this analysis is to validate that the observed frequencies of predicted annotations and mCherry status (tagged vs not tagged) match our expectations. The categories for each nucleus are:

- a. mCherry tagged and EC-amp predicted
- b. not mCherry tagged and EC-amp predicted
- c. mCherry tagged and HSR-amp predicted
- d. not mCherry tagged and HSR-amp predicted

To determine whether a nucleus is mCherry tagged, we took the maximum mCherry brightness over all of the pixels in the segmented nuclei. We classify a nucleus as mCherry tagged if its maximum pixel intensity exceeds 10 pixel brightness. We selected the threshold of 10 pixel brightness as it strikes a balance between precision and recall in the AuC Curve for both HSR-amp and EC-amp cells (Supplementary Figure 16, Supplementary Data 7). Since we used maximum pixel intensity as the threshold, we excluded nuclei near the boundary, as pixels from these nuclei are missing.

Since mCherry is an RFP which is inserted into COLO320DM, we expect only the ecDNA-amp nuclei to be tagged, given 100% mCherry tagging accuracy.

However, the mCherry tagging accuracy is likely lower than 100%, and this analysis aims to estimate the number  $x$  of true ecDNA nuclei that are not mCherry tagged.

Let  $N_h, N_e$  represent the number of nuclei that are not mCherry tagged and are mCherry tagged, respectively.

Let  $(c_h, c_e)$  be the counts of predicted HSR-amp nuclei and EC-amp nuclei which are not mCherry tagged. We observed that interSeg did not predict any of the nuclei in the mCherry tagging experiment as no-amp.

Let  $p_h, p_e$  represent the probabilities of an interSeg prediction (using only the target channel) being HSR-amp and ecDNA-amp respectively, given the cell is truly EC-amp and the interSeg prediction is not no-amp.

Let  $q_h, q_e$  represent the probabilities of an interSeg prediction (using only the target channel) being HSR-amp and EC-amp respectively, given the cell is truly HSR-amp and the interSeg prediction is not no-amp.

Let  $\vec{o}$  represent the observed predictions (EC-amp, HSR-amp) from interSeg for all nuclei.

Let  $\vec{o}_{mCherry (+)}$  represent the interSeg predictions on the subset of nuclei that are mCherry tagged.

Let  $\vec{s}_{mCherry}$  represent the mCherry status (not mCherry tagged / mCherry tagged) for all nuclei.

$$P(\vec{o} | x, \vec{s}_{mCherry}) = P(\vec{o}_{mCherry (+)} | \vec{s}_{mCherry}) \left[ \sum_{a_h=0}^x \frac{x}{a_h} \frac{N_h - x}{c_h - a_h} p_h^{a_h} p_e^{x-a_h} q_h^{c_h - a_h} q_e^{c_e + a_h - x} \right]$$

Since  $P(\vec{o}_{mCherry (+)} | \vec{s}_{mCherry})$  is constant with respect to  $x$

$$\propto \sum_{a_h=0}^x \frac{x}{a_h} \frac{N_h - x}{c_h - a_h} p_h^{a_h} p_e^{x-a_h} q_h^{c_h - a_h} q_e^{c_e + a_h - x}$$

If we assume the prior that all valid values of  $0 \leq x \leq N_h$  are equally likely, then the likelihood  $P(x | \vec{o}, \vec{s}_{mCherry})$  is proportional to the above posterior.

Therefore the maximum likelihood estimate for  $x$  is given by

$$x = \arg \max_{0 \leq x \leq N_h} \sum_{a_h=0}^x \frac{x}{a_h} \frac{N_h - x}{c_h - a_h} p_h^{a_h} p_e^{x-a_h} q_h^{c_h - a_h} q_e^{c_e + a_h - x}$$

In the hybrid images,  $(c_h, c_e) = (309, 28)$

Across our entire COLO320DM\_MYC test dataset,  $(p_h, p_e) = (0.2642, 0.7358)$

Across our entire COLO320HSR\_MYC test dataset,  $(q_h, q_e) = (0.9763, 0.0237)$

The value  $x$ , which represents the number of EC-amp nuclei which are not mCherry tagged, maximizes the above likelihood when  $x=28$  nuclei.

To test this  $x=28$  nuclei prediction, we performed a chi-squared test on the expected vs observed nuclei counts on the 4 categories (mCherry tagging status and interSeg prediction). With a chi-squared test statistic of 2.7252 and a p-value of 0.4360, we observed no statistically significant difference between the distribution of expected vs observed nuclei counts.

Given that 428 / 765 nuclei were mCherry tagged, this would mean that  $28/(428+28)=6.14\%$  percent of true EC-amp were not mCherry tagged. This would therefore set the percentage of true EC-amp nuclei that were thresholded as mCherry tagged at 93.86%.

## Acknowledgements

This work was delivered as part of the eDyNAmiC team supported by the Cancer Grand Challenges partnership funded by Cancer Research UK (CGCATF-2021/100012+ CGCATF-2021/100025) and the National Cancer Institute (OT2CA278688+OT2CA278635). This work is additionally supported by funding from the ARPA-H ADAPT Program (OT 140D042590013). The research was also supported in part by grants U24CA264379, R01GM114362 and Boundless Bio, inc. to VB.

This material is based upon work supported by the National Science Foundation Graduate Research Fellowship Program under Grant No. DGE-2545911. Any opinions, findings, and conclusions or recommendations expressed in this material are those of the author(s) and do not necessarily reflect the views of the National Science Foundation.

X.Y. is a Damon Runyon Fellow supported by the Damon Runyon Cancer Research Foundation (DRG-2474-22). The project described was supported, in part, by Award Number 1S10OD010580-01A1 from the National Center for Research Resources (NCRR). Its contents are solely the responsibility of the authors and do not necessarily represent the official views of the NCRR or the National Institutes of Health. Cell Sciences Imaging Facility provided training and usage support.

S.W. is supported by the Cancer Prevention and Research Institute of Texas (CPRIT) grant RR210034.

A.G.H. is supported by the Deutsche Krebshilfe (German Cancer Aid) Mildred Scheel Professorship program – 70114107. This work was supported by the German Research Foundation (Deutsche Forschungsgemeinschaft DFG) within Collaborative Research Center CRC1588 (493872418) and CRC 1399 (413326622).

### **Conflicts of Interest**

V.B. is a cofounder, paid consultant, and SAB member and has equity interest in Boundless Bio and Abterra Biosciences. The terms of this arrangement have been reviewed and approved by the University of California, San Diego, in accordance with its conflict-of interest policies. H.Y.C. is an employee and stockholder of Amgen. H.Y.C. is a cofounder of Accent Therapeutics, Boundless Bio, Cartography Biosciences, and Orbital Therapeutics and was an advisor of 10x Genomics, Arsenal Biosciences, Chroma Medicine, and Spring Discovery. P.S.M. is a cofounder and advisor of Boundless Bio. S. Wu is a member of the scientific advisory board of Dimension Genomics Inc. The remaining authors declare no competing interests.

### **Data Availability**

All cultured cell line, tissue model, and patient tissue imaging data from our analysis have been made publicly available on Mendeley Data<sup>43</sup>: [doi.org/10.17632/t9vmmjg3zc.1](https://doi.org/10.17632/t9vmmjg3zc.1). This data repository contains metadata files on train-test split information and model weights. We have uploaded all available images and their associated quality score metrics, including images that do not meet our quality score criterion.

The collection and use of patient specimens was approved by the institutional review boards of Charité-Universitätsmedizin Berlin and the Medical Faculty, University of Cologne. Specimens and clinical data were archived and made available by Charité-Universitätsmedizin Berlin or the National Neuroblastoma Biobank and Neuroblastoma Trial Registry (University Children's Hospital Cologne).

### **Code Availability**

InterSeg, interSeg submodules (ecSeg-i and ecSeg-c), and Stat-FISH software are publicly available on GitHub for academic use at <https://github.com/UCRajkumar/ecSeg> (v1.0.0)<sup>44</sup>.

### **Author Contributions**

U.R., G.P., P.S.M., and V.B. conceived the method and designed the experimental strategy to test it and wrote the manuscript. U.R., G.P., and V.B. designed the neural architecture and the computational methodology. E.J.C., I.T.W., X.Y., S.Z., L.B., K.T., J.Wi., J.Wa., H.H., S.W., J.T., M.F., H.Y.C., A.G.H. and P.S.M. designed and executed the experimental strategy. L.B., J.T., M.F., and A.G.H. helped with the analysis and interpretation of the Neuroblastoma dataset. All authors analyzed the results and reviewed the manuscript.

## REFERENCES

1. Beroukhim, R. *et al.* The landscape of somatic copy-number alteration across human cancers. *Nature* **463**, 899–905 (2010).
2. Lockwood, W. W. *et al.* DNA amplification is a ubiquitous mechanism of oncogene activation in lung and other cancers. *Oncogene* **27**, 4615–4624 (2008).
3. Kitada, K. & Yamasaki, T. The complicated copy number alterations in chromosome 7 of a lung cancer cell line is explained by a model based on repeated breakage-fusion-bridge cycles. *Cancer Genet. Cytogenet.* **185**, 11–19 (2008).
4. Raeisi Dehkordi, S. *et al.* Breakage fusion bridge cycles drive high oncogene number with moderate intratumoural heterogeneity. *Nat. Commun.* **16**, 1497 (2025).
5. Turner, K. M. *et al.* Extrachromosomal oncogene amplification drives tumour evolution and genetic heterogeneity. *Nature* **543**, 122–125 (2017).
6. Verhaak, R. G. W., Bafna, V. & Mischel, P. S. Extrachromosomal oncogene amplification in tumour pathogenesis and evolution. *Nat. Rev. Cancer* **19**, 283–288 (2019).
7. Kim, H. *et al.* Extrachromosomal DNA is associated with oncogene amplification and poor outcome across multiple cancers. *Nat. Genet.* **52**, 891–897 (2020).
8. Lange, J. T. *et al.* The evolutionary dynamics of extrachromosomal DNA in human cancers. *Nat. Genet.* **54**, 1527–1533 (2022).
9. Cox, D., Yuncken, C. & Spriggs, A. MINUTE CHROMATIN BODIES IN MALIGNANT TUMOURS OF CHILDHOOD. *The Lancet* **286**, 55–58 (1965).
10. Luebeck, J. *et al.* Extrachromosomal DNA in the cancerous transformation of Barrett's oesophagus. *Nature* **616**, 798–805 (2023).
11. Siu, L. L. & Pugh, T. J. Extrachromosomal DNA — Amping Up Cancer. *N. Engl. J. Med.* **392**, 1447–1450 (2025).
12. Weird rings of DNA fuel cancers. This scientist leads the effort to target them.  
<https://www.science.org/content/article/weird-rings-dna-fuel-cancers-scientist-leads-effort->

target-them.

13. Deshpande, V. *et al.* Exploring the landscape of focal amplifications in cancer using AmpliconArchitect. *Nat. Commun.* **10**, 392 (2019).
14. Luebeck, J. *et al.* AmpliconReconstructor integrates NGS and optical mapping to resolve the complex structures of focal amplifications. *Nat. Commun.* **11**, 4374 (2020).
15. Hadi, K. *et al.* Distinct Classes of Complex Structural Variation Uncovered across Thousands of Cancer Genome Graphs. *Cell* **183**, 197-210.e32 (2020).
16. Pribus, S., Curtis, C., Altman, R. & Houlahan, K. ecDNAInspector: a tool for ecDNA inference quality control, applied in HER2+ Breast Cancer. <https://doi.org/10.25740/js572qn8455> (2024) doi:10.25740/js572qn8455.
17. Wang, S. *et al.* Machine learning-based extrachromosomal DNA identification in large-scale cohorts reveals its clinical implications in cancer. *Nat. Commun.* **15**, 1515 (2024).
18. Repetto, M. *et al.* Abstract 3365: Reliable detection of potentially therapeutically actionable ecDNA using clinical-grade NGS in a large pan-cancer cohort. *Cancer Res.* **84**, 3365 (2024).
19. Nathanson, D. A. *et al.* Targeted Therapy Resistance Mediated by Dynamic Regulation of Extrachromosomal Mutant EGFR DNA. *Science* **343**, 72–76 (2014).
20. Rajkumar, U. *et al.* EcSeg: Semantic Segmentation of Metaphase Images Containing Extrachromosomal DNA. *iScience* **21**, 428–435 (2019).
21. Choudhury, M. *et al.* ecPath detects ecDNA in tumors from histopathology images. 2024.11.13.623494 Preprint at <https://doi.org/10.1101/2024.11.13.623494> (2024).
22. Turner, K. M. *et al.* Extrachromosomal oncogene amplification drives tumour evolution and genetic heterogeneity. *Nature* **543**, 122–125 (2017).
23. Hung, K. L. *et al.* ecDNA hubs drive cooperative intermolecular oncogene expression. *Nature* **600**, 731–736 (2021).
24. Alitalo, K., Schwab, M., Lin, C. C., Varmus, H. E. & Bishop, J. M. Homogeneously

- staining chromosomal regions contain amplified copies of an abundantly expressed cellular oncogene (c-myc) in malignant neuroendocrine cells from a human colon carcinoma. *Proc. Natl. Acad. Sci.* **80**, 1707–1711 (1983).
25. Quinn, L. A., Moore, G. E., Morgan, R. T. & Woods, L. K. Cell Lines from Human Colon Carcinoma with Unusual Cell Products, Double Minutes, and Homogeneously Staining Regions<sup>1</sup>. *Cancer Res.* **39**, 4914–4924 (1979).
  26. Yang, L. *et al.* NuSeT: A deep learning tool for reliably separating and analyzing crowded cells. *PLOS Comput. Biol.* **16**, e1008193 (2020).
  27. Huang, G., Liu, Z., Maaten, L. V. D. & Weinberger, K. Q. Densely Connected Convolutional Networks. in 2261–2269 (IEEE Computer Society, 2017). doi:10.1109/CVPR.2017.243.
  28. Krizhevsky, A., Sutskever, I. & Hinton, G. E. ImageNet Classification with Deep Convolutional Neural Networks. in *Advances in Neural Information Processing Systems* vol. 25 (Curran Associates, Inc., 2012).
  29. Hung, K. L. *et al.* Coordinated inheritance of extrachromosomal DNA species in human cancer cells. *bioRxiv* 2023.07.18.549597 (2023) doi:10.1101/2023.07.18.549597.
  30. Koche, R. P. *et al.* Extrachromosomal circular DNA drives oncogenic genome remodeling in neuroblastoma. *Nat. Genet.* **52**, 29–34 (2020).
  31. Luebeck, J. *et al.* AmpliconSuite: an end-to-end workflow for analyzing focal amplifications in cancer genomes. 2024.05.06.592768 Preprint at <https://doi.org/10.1101/2024.05.06.592768> (2024).
  32. Chamorro González, R. *et al.* Parallel sequencing of extrachromosomal circular DNAs and transcriptomes in single cancer cells. *Nat. Genet.* **55**, 880–890 (2023).
  33. Koche, R. P. *et al.* Extrachromosomal circular DNA drives oncogenic genome remodeling in neuroblastoma. *Nat. Genet.* **52**, 29–34 (2020).
  34. Purshouse, K., Pollard, S. M. & Bickmore, W. A. Imaging extrachromosomal DNA

- (ecDNA) in cancer. *Histochem. Cell Biol.* **162**, 53–64 (2024).
35. Noorani, I. *et al.* Extrachromosomal DNA–Driven Oncogene Spatial Heterogeneity and Evolution in Glioblastoma. *Cancer Discov.* **15**, 2078–2095 (2025).
36. Montuori, G. *et al.* Extrachromosomal DNA–Driven Oncogene Dosage Heterogeneity Promotes Rapid Adaptation to Therapy in MYCN-Amplified Cancers. *Cancer Discov.* **15**, 2054–2077 (2025).
37. Lv, W. *et al.* Spatial–Temporal Diversity of Extrachromosomal DNA Shapes Urothelial Carcinoma Evolution and the Tumor Immune Microenvironment. *Cancer Discov.* **15**, 1225–1246 (2025).
38. Chapman, O. S. *et al.* Circular extrachromosomal DNA promotes tumor heterogeneity in high-risk medulloblastoma. *Nat. Genet.* **55**, 2189–2199 (2023).
39. Tanaka, H. & Watanabe, T. Mechanisms Underlying Recurrent Genomic Amplification in Human Cancers. *Trends Cancer* **6**, 462–477 (2020).
40. Bolzán, A. D., Páez, G. L., Bianchi, M. S. & Bianchi, N. O. Analysis of Telomeric Repeats and Telomerase Activity in Human Colon Carcinoma Cells with Gene Amplification. *Cancer Genet. Cytogenet.* **120**, 166–170 (2000).
41. Roukos, V., Pegoraro, G., Voss, T. C. & Misteli, T. Cell cycle staging of individual cells by fluorescence microscopy. *Nat. Protoc.* **10**, 334–348 (2015).
42. Gibbons-Fideler, I. *et al.* Identification of HER2 Immunohistochemistry-Negative, FISH-Amplified Breast Cancers and Their Response to Anti-HER2 Neoadjuvant Chemotherapy. *Am. J. Clin. Pathol.* **151**, 176–184 (2019).
43. Prasad, G. *et al.* interSeg: Accurate Prediction of ecDNA in Interphase Cancer Cells using Deep Neural Networks [Data set]. Mendeley Data <https://doi.org/10.17632/T9VMMJG3ZC.1> (2025).
44. Prasad, G. & Rajkumar, U. UCRajkumar/ecSeg: v1.0.0. Zenodo <https://doi.org/10.5281/zenodo.18846523> (2026).

## MAIN FIGURE CAPTIONS

**Figure 1: Data overview and Analysis pipeline.** (a) Examples of interphase cells with EC-amp, HSR-amp, No-amp (*MYC* red, Centromere 8 green). (b) Image acquisition protocols for various tissue modalities. (c) Distribution of tissue types and image acquisition protocols in analyzed cell lines and patient tissues, for the training and hold-out test set. Image credits: Pikovit44 (human internal organs) and juliawhite (brain)/iStock via Getty Images.

**Figure 2: Tool pipeline.** (a) InterSeg pipeline with 2 submodules: ecSeg-i and ecSeg-c. TGT: target FISH probe, and CEN: centromeric FISH probe. (b) EcSeg-i architecture based on DenseNet-121.

**Figure 3: Testset results.** (a) InterSeg F1-score on cultured cell line and tissue model test set, where  $n$  is the number of cells in each class. (b) Bootstrapped distribution of interSeg amplification mechanism of no-amp cell lines. (c) Bootstrapped distribution of interSeg amplification mechanism of EC-amp cell lines. (d) Bootstrapped distribution of interSeg amplification mechanism of HSR-amp cell lines. (e) EcSeg-c evaluation on NB hold-out set.

**Figure 4: Explaining amplification mechanism using Stat-FISH.** (a) Image-level mean and variance of copy number signal for HSR-amp and EC-amp images. (b) Number of oncogene foci per cell across all cell lines separated by EC-amp, HSR-amp, and no-amp. (c) Copy number signal per cell across all cell lines separated by EC-amp, HSR-amp, and no-amp. (d) Copy number signal of an EC-amp cell line (SNU16) and a HSR-amp cell line (HCC827) (e) Example of probing multiple oncogenes within a metaphase/interphase spread in H716 (*MYC* red, *FGFR2* green). (f) Number of oncogene foci and copy number signal of *FGFR2* and *MYC* oncogene for each cell in H716.

**Figure 5: Patient Tissue Results.** (a) Non-bootstrapped distribution of interSeg amplification mechanisms across all NB samples with pathologist annotation. The samples were stratified by 'no-amplification' and 'amplification' labels annotated by pathologists. Each column corresponds to a single patient, and the bar height corresponds to the proportion of cells labeled for each amplification class by interSeg. (b) InterSeg predictions on NB test set samples compared with calls based on Amplicon Suite analysis of Whole Genome Sequencing Data.

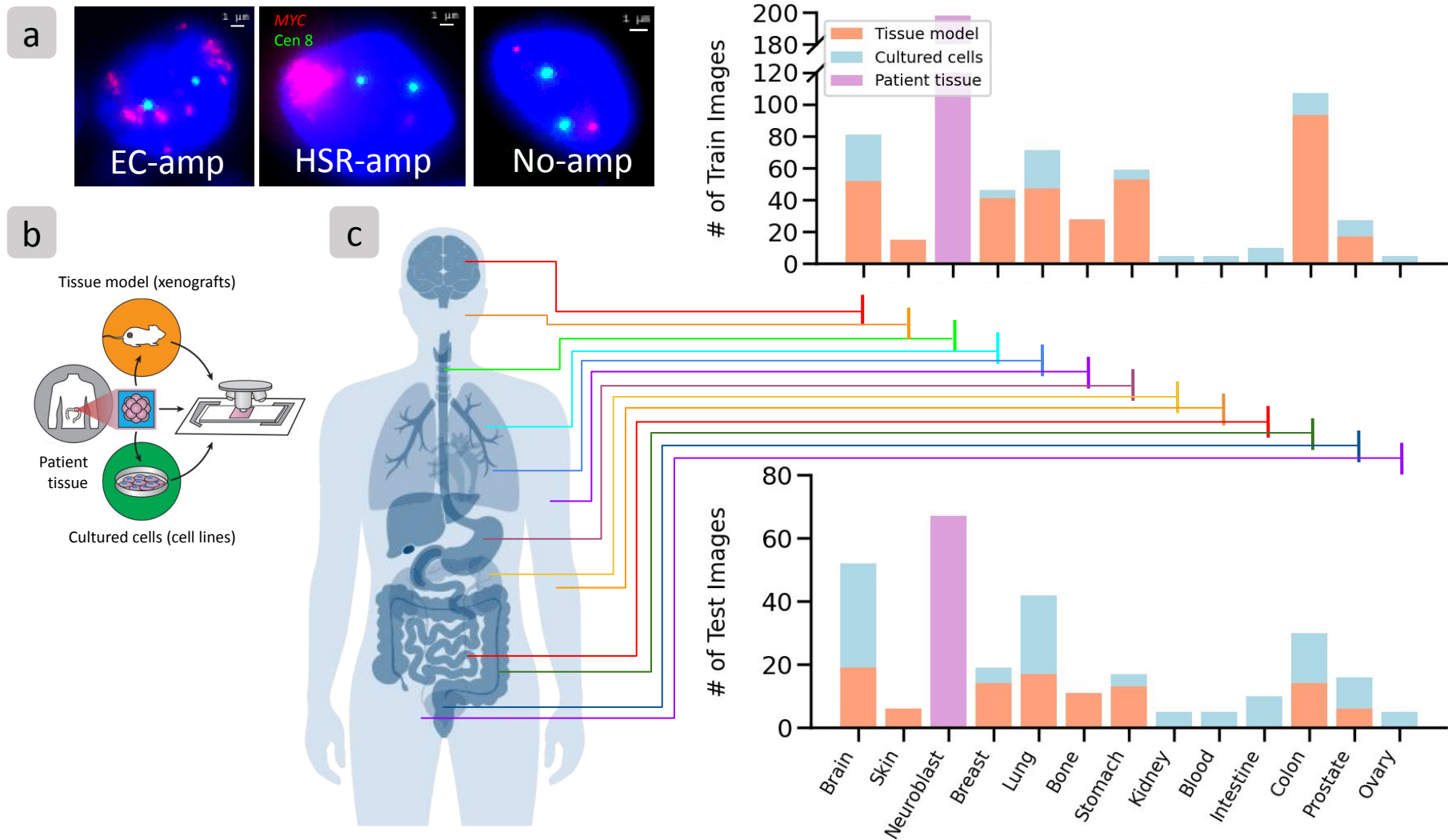
**Editorial Summary:**

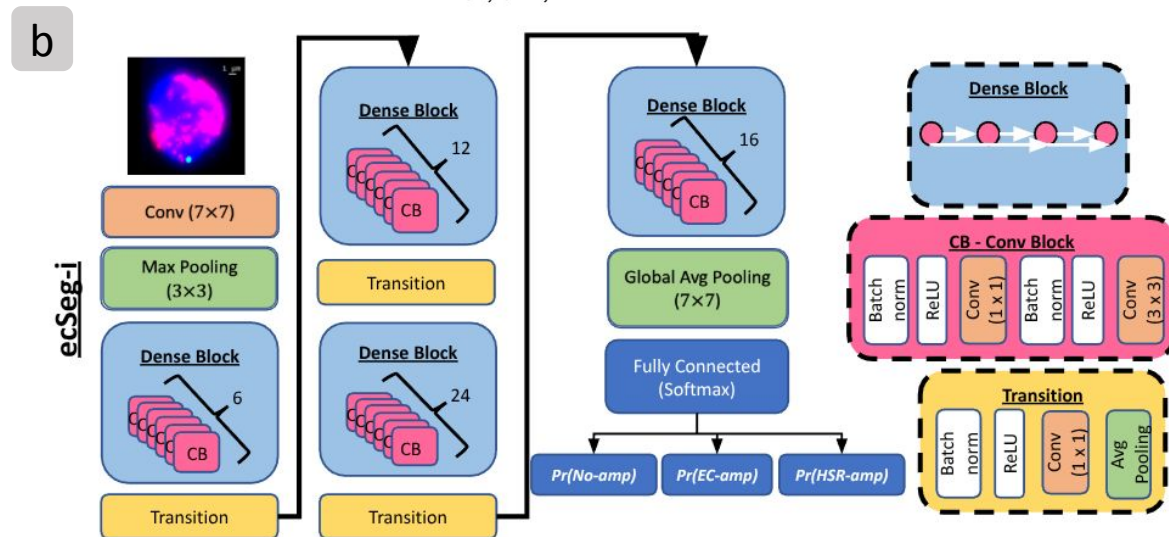
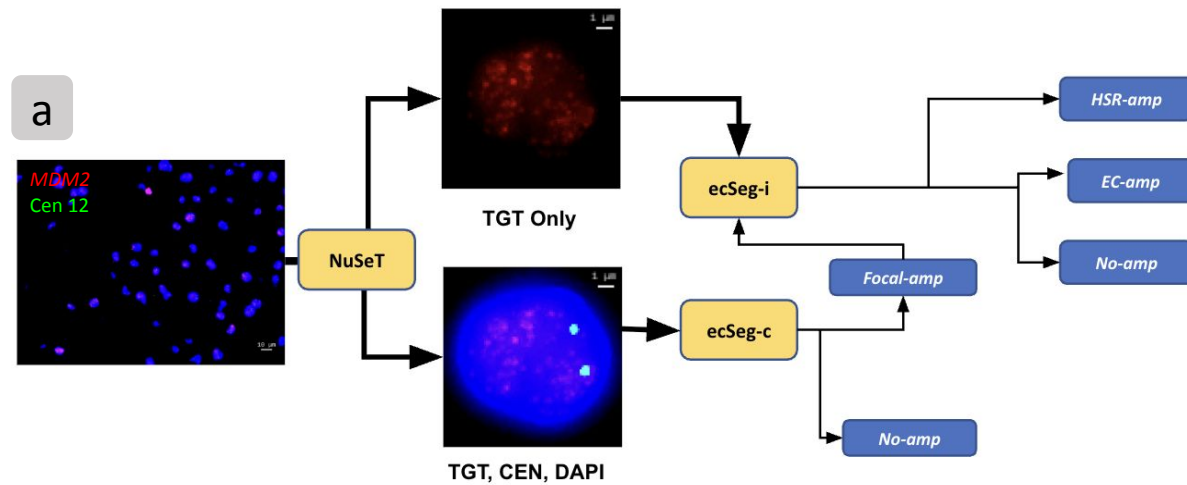
Deep learning-based modeling of interphase DNA-FISH images enables accurate detection of extrachromosomal DNA (ecDNA) across cell lines, xenografts, and patient tissues, overcoming the traditional requirement for mitotic cells in metaphase spreads.

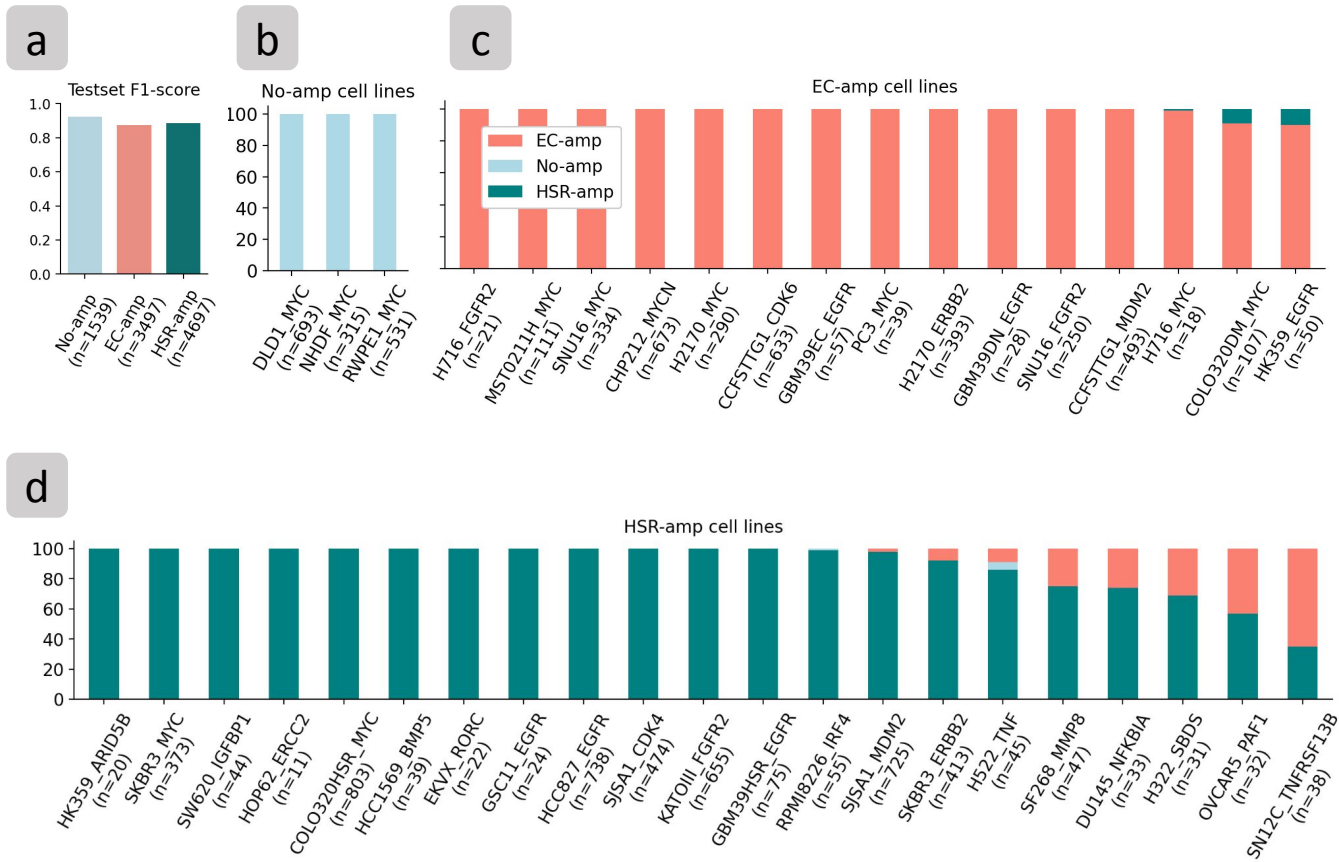
**Peer Review Information:**

*Communications Biology* thanks Hisashi Tanaka and the other, anonymous, reviewer(s) for their contribution to the peer review of this work. Primary Handling Editors: Shan E Ahmed Raza and Mengtan Xing.

ARTICLE IN PRESS





**e**

ecSeg-c prediction	Pathologists report	
	Amplified	No-amp
Amplified	47	0
No-amp	2	18
Total	49	18

